УДК 539.165

LIMITS ON DIFFERENT MAJORON DECAY MODES OF ^{100}Mo, ^{116}Cd, ^{82}Se, AND ^{96}Zr FOR NEUTRINOLESS DOUBLE BETA DECAYS IN THE NEMO-2 EXPERIMENT

V.Vasilyev et al.
(NEMO collaboration[1])

The NEMO-2 tracking detector located in the Fréjus underground laboratory was designed as a prototype for the NEMO-3 detector and to study different modes of double beta decay. Measurements with ^{100}Mo, ^{116}Cd, ^{82}Se, and ^{96}Zr were carried out. Presented here are the experimental half-life limits on double beta decays for new Majoron emission modes and limits on effective neutrino–Majoron coupling constants.

Детектор NEMO-2, расположенный в подземной лаборатории Фреджус и сконструированный как прототип детектора NEMO-3, предназначен для изучения различных мод двойного бета-распада. Были проведены измерения изотопов ^{100}Mo, ^{116}Cd, ^{82}Se и ^{96}Zr. В работе представлены новые экспериментальные пределы на различные моды двойного бета-распада с испусканием майорона и эффективных констант связи нейтрино–майорон.

INTRODUCTION

Spontaneous violation of global $(B-L)$ symmetry in gauge theories leads to the existence of a massless Goldstone boson, the Majoron. At the beginning of the 1980's there were considered to be singlet [1], doublet [2] and triplet [3] Majoron models. All these models resulted in the neutrinoless double beta (2β) decay with the emission of a Majoron (χ^0):

$$(A, Z) \to (A, Z+2) + 2e^- + \chi^0. \quad (1)$$

However, the interaction of the triplet (or doublet) Majorons with the Z^0 boson would give a contribution to the width of the Z^0 decay, which corresponds to two (or 1/2) additional massless neutrino types (see, for example, [4–6]). LEP data gives 2.994 ± 0.012 neutrino types [7], thus triplet and some doublet Majorons are excluded. Nevertheless, in Ref. 8 it is proposed that a small gauge coupling constant does not eliminate the possibility of a large Yukawa coupling with neutrinos. Thus, the singlet and doublet Majorons can still contribute to neutrinoless 2β decay [8, 9].

Another possibility for neutrinoless 2β decay with Majoron emission arises in supersymmetry models with R-parity violation [9, 10]. It was first stated in [10] that there is the possibility of a $2\beta\chi^0\chi^0$ decay with the emission of two Majorons:

$$(A, Z) \to (A, Z+2) + 2e^- + 2\chi^0. \quad (2)$$

[1] The full author list of the collaboration is given at the end of the paper.

In the 1990's several new Majoron models were suggested. The term «Majoron» here denotes massless or light bosons with a coupling to neutrinos. In these models Majoron can carry a lepton charge, but cannot be a Goldstone boson [11]. Additionally there can be decays with the emission of two Majorons [12]. In the models with a vector Majoron it is a longitudinal component of the massive gauge boson emitted in 2β decay [13]. All these new objects are called Majorons for simplicity.

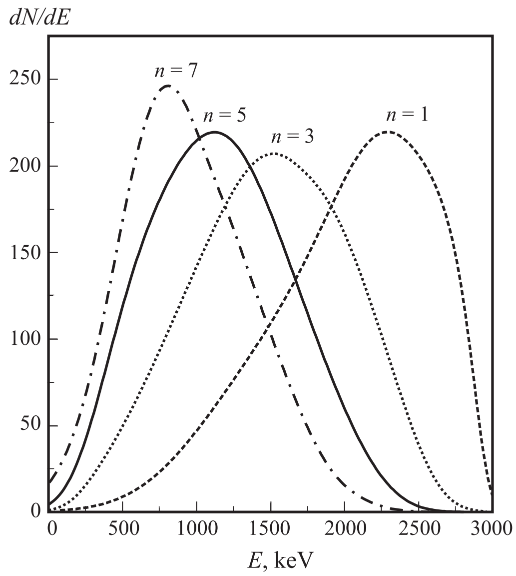

Fig. 1. Energy spectra of different modes of $2\beta2\nu$ $(n = 5)$, $2\beta\chi^0$ $(n = 1$ and $3)$ and $2\beta\chi^0\chi^0(n =$ 3 and 7) decays of ^{100}Mo

Table 1. **Different Majoron models according to [12,14]. The mode IIF corresponds to the model of C.D.Carone [13]**

Case	Decay mode	Goldstone boson	L	n	Matrix element
IB	$2\beta\chi^0$	no	0	1	$M_F - M_{GT}$
IC	$2\beta\chi^0$	yes	0	1	$M_F - M_{GT}$
ID	$2\beta\chi^0\chi^0$	no	0	3	$M_{F\omega^2} - M_{GT\omega^2}$
IE	$2\beta\chi^0\chi^0$	yes	0	3	$M_{F\omega^2} - M_{GT\omega^2}$
IIB	$2\beta\chi^0$	no	-2	1	$M_F - M_{GT}$
IIC	$2\beta\chi^0$	yes	-2	3	M_{CR}
IID	$2\beta\chi^0\chi^0$	no	-1	3	$M_{F\omega^2} - M_{GT\omega^2}$
IIE	$2\beta\chi^0\chi^0$	yes	-1	7	$M_{F\omega^2} - M_{GT\omega^2}$
IIF	$2\beta\chi^0$	gauge boson	-2	3	M_{CR}

In Table 1 there are nine Majoron models presented (following [12–14]), which are considered in this work. It is divided into two sections, one for lepton number violation and one for lepton number conserving models. The table also shows whether the corresponding

2β decay is accompanied by the emission of one or two Majorons. The next three entries list the main features of the models: the third column lists whether the Majoron is a Goldstone boson or not (or a gauge boson in the case of vector Majorons, type IIF). In column four the leptonic charge L is given. Column five gives the «spectral index» n of the summed energy of the emitted electrons, which is defined by the phase space of the emitted particles, $G \sim (Q_{\beta\beta} - T)^n$. Here $Q_{\beta\beta}$ is the energy released in the decay; and T, the energy of the two electrons. Energy spectra of different modes of $2\beta 2\nu$ $(n = 5)$, $2\beta\chi^0$ $(n = 1$ and $3)$ and $2\beta\chi^0\chi^0$ $(n = 3$ and $7)$ decays are presented in Fig. 1. The different shapes can be used to distinguish the different Majoron decay modes from each other and 2β decay with the emission of two neutrinos. In the last column of Table 1 the nuclear matrix elements (NME) are listed.

Attempts to observe 2β decay with Majoron emission have been undertaken for the last 20 years. Consequently there now exist strong limits on the «standard» Majoron with the «standard» electron energy spectrum shape $(n = 1)$, see Table 2. The best limits on the Majoron coupling constant $(\langle g_{ee} \rangle)$ were obtained in experiments with ^{128}Te [15], ^{116}Cd [16], ^{100}Mo [17], and ^{136}Xe [27] yielding a limit on $\langle g_{ee} \rangle$ on the level $\sim 10^{-4}$. Sufficiently less information exists for «nonstandard» Majoron models. The most carefully studied «nonstandard» models are being investigated with ^{76}Ge [18]. There are also limits on decays with the emission of two Majorons in ^{100}Mo [19] and ^{116}Cd [20].

Table 2. **Summary of the best results on the $2\beta\chi^0$ decay with $n = 1$. All limits are presented at the 90 % C.L. The dispersion of $\langle g_{ee} \rangle$ values is due to uncertainties in the NME calculation. The NME from the following works were used: ^{48}Ca — [29–31], ^{150}Nd — [32–35], and others — [16, 24, 31, 33–37]**

Nucleus	$T_{1/2}$, y	$\langle g_{ee} \rangle$, 10^{-4}
^{48}Ca	$> 7.2 \cdot 10^{20}$ [25]	$< (5.3{-}8.8)$
^{76}Ge	$> 7.9 \cdot 10^{21}$ [26]	$< (2.6{-}7.5)$
^{82}Se	$> 2.4 \cdot 10^{21}$ [23]	$< (2.3{-}4.3)$
^{96}Zr	$> 3.9 \cdot 10^{20}$ [24]	$< (2.6{-}4.9)$
^{100}Mo	$> 3.1 \cdot 10^{21}$ [17]	$< (1{-}4.3)$
^{116}Cd	$> 1.2 \cdot 10^{21}$ [16]	$< (1.2{-}4.4)$
^{128}Te	$> 2 \cdot 10^{24}$ (geochemical) [15]	$< (0.7{-}1.4)$
^{130}Te	$> 0.8 \cdot 10^{21}$ (geochemical) [15]	$< (2.8{-}6.8)$
^{136}Xe	$> 7.2 \cdot 10^{21}$ [27]	$< (1.3{-}3.8)$
^{150}Ne	$> 2.8 \cdot 10^{20}$ [28]	$< (1{-}5.4)$

In this work a systematic search for 2β decays with different Majoron types was carried out for ^{100}Mo, ^{116}Cd, ^{82}Se, and ^{96}Zr, using the experimental data obtained with the NEMO-2 detector [21]. Limits on the standard Majoron $(n = 1)$ were published earlier [16, 22–24].

1. NEMO-2 DETECTOR

The NEMO-2 detector (Fig. 2) consists of a 1 m^3 tracking volume filled with helium gas and 4 % ethyl alcohol. Vertically bisecting the detector is the plane of the source foil

(1 × 1 m). Tracking is accomplished with long open Geiger cells with an octagonal cross section defined by 100 μm nickel wires. On each side of the source foil there are 10 planes of 32 cells which alternate between vertical and horizontal orientations. Collectively the cells provide three-dimensional tracking of charged particles.

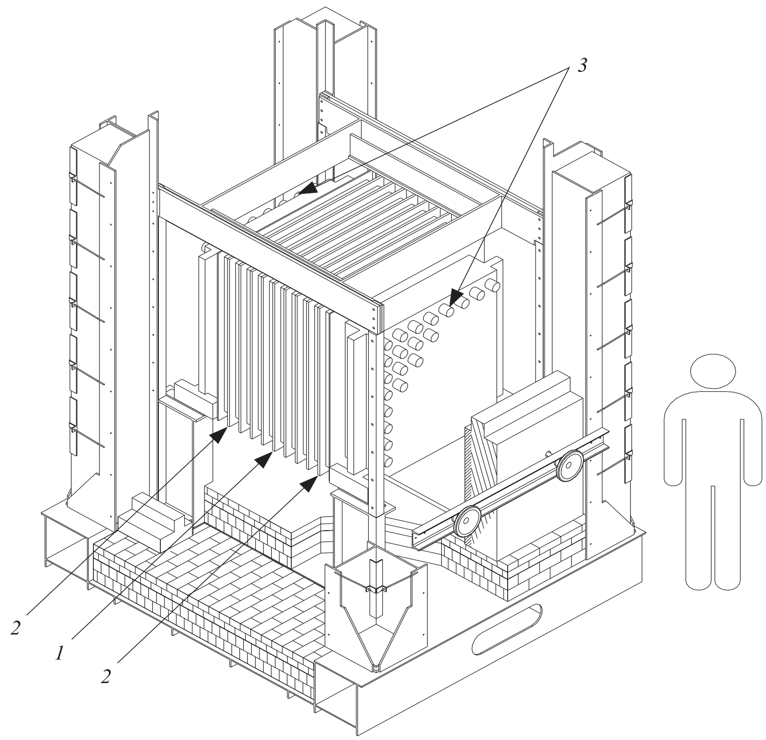

Fig. 2. The NEMO-2 detector without shielding: *1* — central frame with the source plane capable of supporting plural source foils; *2* — ten frames of 2×32 Geiger cells for tracking; *3* — scintillator array

A calorimeter made of scintillators covers two vertical opposing sides of the tracking volume. It consisted of two planes of 64 scintillators for the ^{100}Mo measurements and 25 scintillators for the ^{116}Cd, ^{82}Se and ^{96}Zr measurements ($12\times12\times2.25$ cm and $19\times19\times10$ cm, respectively). In the last case low-radioactivity photomultipliers tubes (PMT) were used. Finally, the tracking volume and scintillators were surrounded by a lead (5 cm) and iron (20 cm) shield.

1.1. Performance. Details of the performances and parameters of NEMO-2 are described elsewhere [16, 21–24] while the most salient characteristics are briefly outlined here. As mentioned above, the three-dimensional measurements of charged particle tracks are provided by the array of Geiger cells. The transverse position is given by the drift time and the longitudinal position by the plasma propagation times. The transverse resolution is 500 μm and the longitudinal resolution is 4.7 mm. Track reconstruction is accomplished with the tracking method based on the Kalman filter [38]. The calorimeter energy resolution (FWHM) is 18 % at 1 MeV with a time resolution of 275 ps (550 ps at 0.2 MeV). A laser and fiber optics device is used to check the stability of the scintillation detectors.

1.2. Event Definition. An electron is defined by a track linking the source foil and one scintillator. The maximum scattering angle along the track has to be less than 20° to reject hard scattering situations. A photon is recognized as one or two adjacent fired scintillators without an associated particle track. For photons and electrons an energy deposited greater than 200 keV is required in order to obtain sufficiently good time resolution. The two-electron events are defined by two tracks which have a common vertex and are associated with two fired scintillators with a deposited energy of at least 200 keV in each one. In the analysis, a two-electron event is identified as $(2e)$; an electron-photon event, as $(e\gamma)$. A more detailed description of the analysis procedure can be found in Refs. 16, 22–24.

1.3. Source-Foils Parameters. Natural (163 g) and ^{100}Mo enriched (172 g) molybdenum metallic foils were manufactured using a standard rolling technology. They were studied in the first experiment. The enriched and natural foils each defined half of the central plane. The second experiment used natural (143 g) and ^{116}Cd enriched (152 g) cadmium metallic foils. The third experiment involved selenium and zirconium sources, which were composed of strips that were produced using a special technique to deposit the material with a binder on mylar films. Masses of enriched materials were $m_{\rm Se} = 157$ g and $m_{\rm Zr} = 20.5$ g and natural were $m_{\rm Se} = 134$ g and $m_{\rm Zr} = 18.3$ g. The Se was placed in the outer region of the central plane and Zr foils in the inner portion of the central plane. The thicknesses of the foils were approximately 40–50 $\text{mg}\cdot\text{cm}^{-2}$ for all foils.

Values of the different contaminations in the foils were obtained with the NEMO-2 detector by analysing electron-gamma and single-electron events, as explained in the sections devoted to backgrounds. These results were compared with HPGe detector measurements.

2. BACKGROUNDS

Backgrounds for the NEMO-2 detector had «internal» and «external» origins. Events connected with natural samples were used to estimate the external background in the enriched samples.

The «external» background is due to photons coming from outside of the tracking detector and interacting with the source foils or with the scintillators. Compton electrons produced in the scintillators and crossing the tracking device were rejected by time-of-flight analysis. Compton electrons produced in the source foils can generate a secondary electron by Möller scattering. A double Compton effect or pair production is also seen as a $2e$ event (NEMO-2 could not distinguish between e^+ and e^-). These $2e$ background events cannot be rejected by time-of-flight cuts. The dominant contribution to the external background comes from the flux of photons emitted by radon located between the tracking detector and the shielding. Another source of background is due to the flux of photons emitted by the PMTs.

Radioactive pollution in the source foils produces a background identified as «internal». An electron which gives rise to the Möller effect, or is associated with an internal conversion electron, or a Compton electron can produce a $2e$ background event.

The main part of the $2e$ background events are due to Möller scattering which leads mainly to small angles between the two electrons. This is not the case for $2\beta2\nu$ decay, where the angles are wide. To improve the signal-to-background ratio the cut $\cos(\theta_{12}) < 0.6$ on the angle between two electrons, (θ_{12}), was applied in the $2e$ event selection for the measurements with ^{116}Cd, ^{82}Se, and ^{96}Zr. Unfortunately the raw data of ^{100}Mo experiment were not saved, and the data were analyzed without this cut.

Since the enriched samples of ^{100}Mo, ^{116}Cd, and ^{82}Se were rather pure the major part of the background in that experiments is of «external» origin. This is not the case with the ^{96}Zr where the background is most of «internal» origin. More thoroughly the problem of the backgrounds is considered in previous works [16, 22–24].

3. EXPERIMENTAL RESULTS

3.1. Analysis Methods of Experimental Data. The experimental data from enriched samples are shown in Fig. 3 as solid line histograms. The sums of external and internal backgrounds for the different experiments are presented as dashed line histograms. The detection efficiencies for the decays depend on the energy of the electrons and were calculated for all four nuclei, for all the Majoron modes (spectral indices $n = 1, 3$ and 7) and for the double beta-decay $(n = 5)$ by a Monte-Carlo simulations with the GEANT 3.21 code.

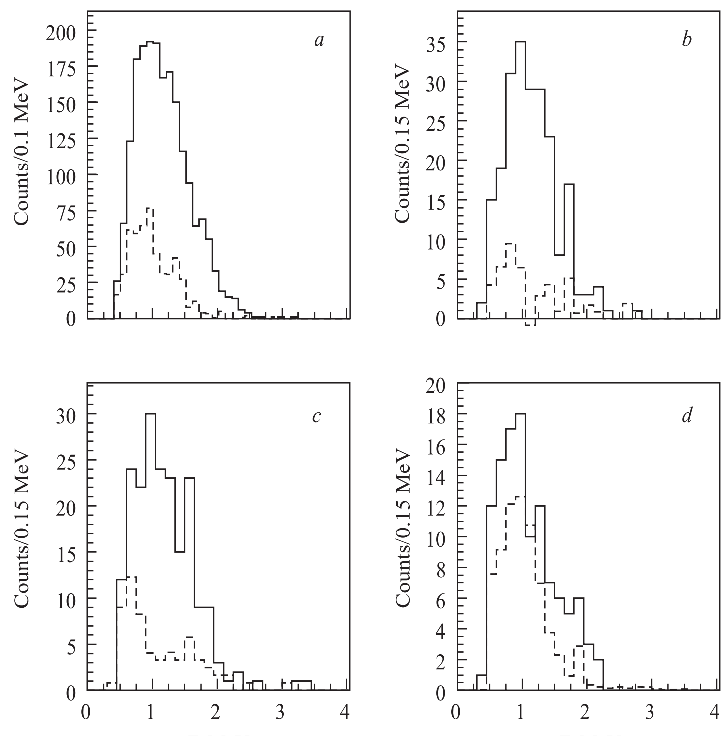

Fig. 3. The $2e$ events (solid line) and estimated backgrounds (dashed line) for ^{100}Mo (a), ^{116}Cd (b), ^{82}Se (c), and ^{96}Zr (d)

Obtaining of limits on the different modes was performed by two methods. In the first one we estimated $T_{1/2}^{2\beta 2\nu}$ from our measurements. Then one can get limits on the Majoron mode if the $2\beta2\nu$ and background are known and used as expected averages in the Helene formula [39] for Poisson processes:

$$CL(N) = 1 - \mathrm{e}^{-(\mu_b+N)} \sum_{n=0}^{n_0} \frac{(\mu_b+N)^n}{n!} / \mathrm{e}^{-\mu_b} \sum_{n=0}^{n_0} \frac{\mu_b^n}{n!}, \qquad (3)$$

where μ_b is the expected average number of events in an interval and is defined by the sum of $2\beta2\nu$ and background events; n_0 is the number of observed events in the same interval; and N is the limit on the mean number of events from a signal. The dependent variable in this equation is the parameter N while the $CL(N)$ is fixed at 90 %.

If one considers the existence of both $2\beta2\nu$ and Majoron decay modes, then the $T_{1/2}^{2\beta2\nu}$ estimation should not depend on the existence or absence of decays with the emission of χ^0. This is applicable for $2\beta\chi^0$ with spectral index $n = 1$, where the $2\beta2\nu$ and Majoron spectra profiles peak in different energy regions (Fig. 1). This was done in previous works [16,22–24]. Results for all nuclei are given in Table 3.

Table 3. **Limits on $T_{1/2}$(y) at 90 % C.L. for decays with Majoron emission, estimated via the Helene formula**

Nucleus	^{100}Mo	^{116}Cd	^{82}Se	^{96}Zr
$n = 1$	$> 5.0 \cdot 10^{20}$ [22]	$> 1.2 \cdot 10^{21}$ [16]	$> 2.4 \cdot 10^{21}$ [23]	$> 3.5 \cdot 10^{20}$ [24]
$n = 3$	$> 9.9 \cdot 10^{19}$	$> 4.6 \cdot 10^{20}$	$> 1.1 \cdot 10^{21}$	$> 6.3 \cdot 10^{19}$
$n = 7$	$> 1.7 \cdot 10^{20}$	$> 2.0 \cdot 10^{20}$	$> 3.7 \cdot 10^{20}$	$> 5.1 \cdot 10^{19}$

Also shown, for comparison only, are the calculations by the Helene formula method for modes with other spectral indices.

In the case when shapes of the spectra are similar, one cannot use the Helene formula, and should follow another method. If one considers the Majoron modes as existing decay channels similar to $2\beta2\nu$, then the experiment is the sum of two processes, $2\beta2\nu$ decay and decay with χ^0 emission. Thus, one cannot know the expected number of $2\beta2\nu$ decays and should set a limit on the decays with Majoron emission by analysing the deviation in the shape of the experimental data calculated for $2\beta2\nu$ decay. This can be done with the likelihood function.

Here the experimental spectrum was again treated as a histogram. One then needs to take into account that the distribution of the events in each bin is a Poisson one and independent of the others. Thus, one constructs the likelihood function as:

$$L(N_\beta, N_\chi) = \prod_{i=n_1}^{n_2} \frac{\mathrm{e}^{-(N_\beta\eta_{\beta i}+N_\chi\eta_{\chi i}+N_{\mathrm{bgr}\,i})}}{N_{\exp\ i}!} (N_\beta\eta_{\beta i} + N_\chi\eta_{\chi i} + N_{\mathrm{bgr}\,i})^{N_{\exp\ i}}, \qquad (4)$$

where n_1 and n_2 are the bin numbers of the energy interval; $N_{\exp\ i}$ is the number of experimental events in the i-th bin; $N_{\mathrm{bgr}\,i}$ is the expected number of background events; and $\eta_{\beta i}$ and $\eta_{\chi i}$ are the Monte-Carlo simulated efficiencies of $2\beta2\nu$ and Majoron decays in the i-th bin. Finally, N_β and N_{χ^0} are the average numbers of decays and they are considered as free parameters.

To find the confidence level for the upper limit on the mean number of decays with Majoron emission ($N_{\chi\mathrm{up}}$) this function (4) has to be normalized and then integrated over all possible values of N_β and N_χ from 0 to $N_{\chi\mathrm{up}}$:

$$CL(N_{\chi\mathrm{up}}) = \frac{\int_0^{N_{\chi\mathrm{up}}} dN_\chi \int_0^\infty dN_\beta\, L(N_\beta, N_\chi)}{\int_0^\infty dN_\chi \int_0^\infty dN_\beta\, L(N_\beta, N_\chi)}. \tag{5}$$

Again, this is an equation for the free parameter $N_{\chi\mathrm{up}}$, where $CL(N_{\chi\mathrm{up}})$ is fixed. To simplify the calculation in the case of ^{100}Mo, for bins with a large number of the events (> 14 events) the Poisson distribution was replaced by a Gaussian distribution. The results are presented in Table 4.

Table 4. **Limits on $T_{1/2}$ at 90 % C.L. for decays with Majoron emission, estimated with the help of likelihood function**

Nucleus	^{100}Mo	^{116}Cd	^{82}Se	^{96}Zr
$n = 1$	$> 6.0 \cdot 10^{20}$	$> 9.2 \cdot 10^{20}$	$> 2.3 \cdot 10^{21}$	$> 3.1 \cdot 10^{20}$
$n = 3$	$> 1.6 \cdot 10^{20}$	$> 3.5 \cdot 10^{20}$	$> 6.3 \cdot 10^{20}$	$> 6.3 \cdot 10^{19}$
$n = 7$	$> 4.1 \cdot 10^{19}$	$> 4.1 \cdot 10^{19}$	$> 1.1 \cdot 10^{20}$	$> 2.4 \cdot 10^{19}$

3.2. Results and Discussion. The half-life limits for different isotopes and decay modes are presented in Tables 3 and 4. Using the half-lives one can get limits on the coupling constants for different Majoron models via the relations (6) and (7).

$$T_{1/2}^{-1} = |\langle \mathrm{g}_{ee} \rangle|^2 |M|^2 G \text{ for } 2\beta\chi^0, \tag{6}$$

$$T_{1/2}^{-1} = |\langle \mathrm{g}_{ee} \rangle|^4 |M|^2 G \text{ for } 2\beta\chi^0\chi^0. \tag{7}$$

The relevant matrix elements M and values of phase spaces G are presented in Tables 5 and 6. Using the data from Table 4 the limits on the coupling constants are calculated and presented in Table 7. In addition, the limits on Majoron-neutrino coupling constants obtained in the ^{76}Ge experiment [18] are presented. Note that for ^{100}Mo and ^{116}Cd there were also limits obtained on decays with two Majorons emission ($n = 3$) for which the limits are $> 5.3 \cdot 10^{19}$ y (68 % C.L.) [19] and $> 2.6 \cdot 10^{20}$ y (90 % C.L.) [20], respectively.

To summarize the results reported here more thoroughly one can note the following. For ^{100}Mo the limit on decays with $n = 3$ obtained here is three times higher than that in [19], while the limit on decays with $n = 7$ is given for the first time. The result for $n = 1$ [22] is several times lower than in [17].

The limit on ^{116}Cd decays with $n = 3$ is two times higher than that in [20]. The limit on decays with $n = 7$ is presented for the first time. The limit on decays with Majoron emission for $n = 1$, obtained in [20], coincides with the results of our earlier work [16].

Next, for ^{96}Zr all the limits are presented for the first time in a direct counting experiment. They can be compared with the geochemical experiments, which give a half-life, $T_{1/2} =$

Table 5. **The pn-QRPA nuclear matrix elements for different nuclei. For ^{82}Se, ^{100}Mo, and ^{116}Cd NME are taken from [18]. For ^{96}Zr the $M_F - M_{GT}$ is presented in [24], the M_{CR} value is the lowest among the other nuclei which is taken as a conservative estimation, and for the $M_{F\omega^2} - M_{GT\omega^2}$ used the same estimate as for the other nuclei in [18]**

Nucleus	$M_F - M_{GT}$	M_{CR}	$M_{F\omega^2} - M_{GT\omega^2}$
^{82}Se	4.03	0.14	10^{-3}
^{100}Mo	4.86	0.16	10^{-3}
^{116}Cd	3.29	0.10	10^{-3}
^{96}Zr	5.58	0.10	10^{-3}

Table 6. **Phase-space integrals (G [y $^{-1}$]) for different nuclei and models of decay [18]. Zr phase space for $n = 1$ is taken from [40], and for $n = 3$ and 7 it is calculated following the formulas of [14]**

Nucleus	$2\beta\chi^0$, $n = 1$	$2\beta\chi^0$, $n = 3$	$2\beta\chi^0\chi^0$,$n = 3$	$2\beta\chi^0\chi^0$, $n = 7$
^{82}Se	$1.03 \cdot 10^{-15}$	$3.49 \cdot 10^{-18}$	$1.01 \cdot 10^{-17}$	$7.73 \cdot 10^{-17}$
^{100}Mo	$1.80 \cdot 10^{-15}$	$7.28 \cdot 10^{-18}$	$1.85 \cdot 10^{-17}$	$1.54 \cdot 10^{-16}$
^{116}Cd	$1.75 \cdot 10^{-15}$	$6.95 \cdot 10^{-18}$	$1.60 \cdot 10^{-17}$	$1.03 \cdot 10^{-16}$
^{96}Zr	$1.24 \cdot 10^{-15}$	$1.07 \cdot 10^{-17}$	$2.81 \cdot 10^{-17}$	$3.26 \cdot 10^{-16}$

Table 7. **Limits on the Majoron coupling constant $\langle g_{ee}\rangle$ at the $90\,\%$ C.L. for ^{82}Se, ^{96}Zr, ^{100}Mo, and ^{116}Cd. ^{76}Ge results are presented for comparison**

Model	Mode	n	^{82}Se	^{96}Zr	^{100}Mo	^{116}Cd	^{76}Ge [18]
IB	$2\beta\chi^0$	1	$< 1.6 \cdot 10^{-4}$	$< 2.6 \cdot 10^{-4}$	$< 2.0 \cdot 10^{-4}$	$< 2.1 \cdot 10^{-4}$	$< 2.3 \cdot 10^{-4}$
IC	$2\beta\chi^0$	1	$< 1.6 \cdot 10^{-4}$	$< 2.6 \cdot 10^{-4}$	$< 2.0 \cdot 10^{-4}$	$< 2.1 \cdot 10^{-4}$	$< 2.3 \cdot 10^{-4}$
IIB	$2\beta\chi^0$	1	$< 1.6 \cdot 10^{-4}$	$< 2.6 \cdot 10^{-4}$	$< 2.0 \cdot 10^{-4}$	$< 2.1 \cdot 10^{-4}$	$< 2.3 \cdot 10^{-4}$
ID	$2\beta\chi^0\chi^0$	3	< 3.5	< 4.7	< 4.3	< 3.6	< 4.1
IE	$2\beta\chi^0\chi^0$	3	< 3.5	< 4.7	< 4.3	< 3.6	< 4.1
IIC	$2\beta\chi^0$	3	< 0.15	< 0.36	< 0.19	< 0.20	< 0.18
IID	$2\beta\chi^0\chi^0$	3	< 3.5	< 4.7	< 4.3	< 3.6	< 4.1
IIF	$2\beta\chi^0$	3	< 0.15	< 0.36	< 0.19	< 0.20	< 0.18
IIE	$2\beta\chi^0\chi^0$	7	< 3.3	< 3.2	< 3.6	< 3.9	< 3.3

$(3.9 \pm 0.9) \cdot 10^{19}$ y. This result is treated as a half-life for $2\beta2\nu$, while $T_{1/2} > 3 \cdot 10^{19}$ y should be treated as a limit on all possible transitions ^{96}Zr→^{96}Mo, such as those involving Majoron emission processes. The NEMO-2 limits exceed those obtained from geochemical experiments for all types of decays with Majoron emission ($n = 1, 3$ and 7).

Finally, the ^{82}Se results for $n = 3$ and 7 are presented here for the first time. Note that the result for the transition with $n = 1$ [23] is also the most stringent for ^{82}Se. Analysis of the results documented above shows that the best limits on the coupling constant for all «nonstandard» decays with Majoron emission ($n = 3$ and 7) were obtained with the NEMO-2 experiment with ^{82}Se.

CONCLUSION

Though NEMO-2 was developed as a prototype for NEMO-3 [41], the limits obtained on 2β-decay processes with Majoron emission are good enough. In particular limits on «nonstandard» Majoron with $n = 3$ and 7 are more stringent than the limits coming from other experiments. The current plan is to start measurements with the NEMO-3 detector at the end of the year 2000. The total mass of the 2β sources will be increased to 10–15 kg, and different isotopes (^{100}Mo, ^{82}Se, ^{116}Cd, ^{130}Te, ^{150}Nd, and ^{96}Zr) will be investigated. The sensitivity to half-life measurments for processes with Majoron emission ($n = 1, 3$ and 7) will be improved by 10 to 100 times, while the limits on the coupling constant will be improved by 3 to 10 times, depending on the type of decay.

Acknowledgement. The authors would like to thank the Fréjus underground laboratory staff for their technical assistance in running the experiment, and are very thankful to V.I.Tretyak for coding new Majoron decay modes. Portions of this work were supported by the Russian Foundation for Branch Investigations (RFBI) under contract 97-02-17344, by INTAS under grant 96-0589 and by US, Department of Energy Grant DE-FG02-90ER40553.

REFERENCES

1. *Chikashige Y., Mohapatra R.N., Peccei R.D.* // Phys. Rev. Lett. 1980. V.45. P.1926; Phys. Lett. B. 1981. V.98. P.265.
2. *Aulakh C., Mohapatra R.* // Phys. Lett. B. 1982. V.119. P.136.
3. *Gelmini G., Roncadelli M.* // Phys. Lett. B. 1981. V.99. P.1411.
4. *Georgi H.M., Glashow S.L., Nussinov S.* // Nucl. Phys. B. 1981. V.193. P.297.
5. *Barger V. et al.* // Phys. Rev. D. 1982. V.26. P.218.
6. *Deshpande N.G.* // Proc. of Conf. on Neutrino Masses and Neutrino Astrophysics / Ed. V.Barger et al. Singapore, 1987. P.78.
7. *Caso C. et al.* (Particle Data Group) // Europ. Phys. J. C. 1998. V.3. P.1.
8. *Berezhiani Z.G., Smirnov A.Yu., Valle J.W.F.* // Phys. Lett. B. 1992. V.291. P.99.
9. *Mohapatra R.N., Pal P.B.* Massive Neutrinos in Physics and Astrophysics. Singapore: World Scientific, 1991.
10. *Mohapatra R.N., Takasugi E.* // Phys. Lett. B. 1998. V.211. P.192.
11. *Burgess C.P., Cline J.M.* // Phys. Lett. B. 1993. V.298. P.141; Phys. Rev. D. 1994. V.49. P.5925.
12. *Bamert P., Burgess C.P., Mohapatra R.N.* // Nucl. Phys. B. 1995. V.449. P.25.
13. *Carone C.D.* // Phys. Lett. B. 1993. V.308. P.85.

14. *Hirsch M. et al.* // Phys. Lett. B. 1996. V.372. P.8.
15. *Manuel O.K.* // J. Phys. G. 1991. V.17. P.221.
16. *Arnold R. et al.* // Z. Phys. C. 1996. V.72. P.239.
17. *Ejiri H. et al.* // Nucl. Phys. A. 1996. V.611. P.85.
18. *Gunther M. et al.* // Phys. Rev. D. 1996. V.54. P.3641.
19. *Tanaka J., Ejiri H.* // Phys. Rev. D. 1993. V.48. P.5412.
20. *Danevich F.A. et al.* // Nucl. Phys. A. 1998. V.643. P.317.
21. *Arnold R. et al.* // Nucl. Instr. Meth. A. 1995. V.354. P.338.
22. *Dassie D. et al.* // Phys. Rev. D. 1995. V.51. P.2090.
23. *Arnold R. et al.* // Nucl. Phys. A. 1998. V.636. P.209.
24. *Arnold R. et al.* // Nucl. Phys. A. 1999. V.658. P.299.
25. *Barabash A.S.* // Phys. Lett. B. 1989. V.216. P.257.
26. *Gunther M. et al.* // Phys. Rev. D. 1997. V.55. P.54.
27. *Luescher R. et al.* // Phys. Lett. B. 1998. V.434. P.407.
28. *De Silva A. et al.* // Phys. Rev. C. 1997. V.56. P.2451.
29. *Haxton W.C., Stephenson G.S.* // Prog. Part. Nucl. Phys. 1984. V.12. P.409.
30. *Retamosa J., Caurier E., Nowacki F.* // Phys. Rev. C. 1995. V.51. P.371.
31. *Caurier E. et al.* // Nucl. Phys. A. 1999. V.654. P.973c.
32. *Hirsch J.G., Castanos O., Hess P.O.* // Nucl. Phys. A. 1995. V.582. P.124.
33. *Muto K., Bender E., Klapdor H.V.* // Z. Phys. A. 1989. V.334. P.187.
34. *Tomoda T.* // Rep. Prog. Phys. 1991. V.54. P.53.
35. *Simkovic F. et al.* // Phys. Rev. C. 1999. V.60. P.055502.
36. *Engel J., Vogel P., Zirnbauer M.R.* // Phys. Rev. C. 1988. V.37. P.73.
37. *Caurier E. et al.* // Phys. Rev. Lett. 1996. V.77. P.1954.
38. *Billoir P.* // Nucl. Instr. Meth. A. 1984. V.255. P.352.
39. *Helene O.* // Nucl. Instr. Meth. B. 1983. V.212. P.319; Particle Data Group // Phys. Rev. D. 1994. V.50. P.1281.
40. *Suhonen J., Civitarese O.* // Phys. Rep. 1998. V.300. P.123.
41. NEMO-3 Proposal. LAL preprint 94-29. 1994.

The NEMO collaboration includes: R.Arnold[j], C.Augier[h], J.Baker[e], A.Barabash[g 1], D.Blum[h], V.Brudanin[c], A.J.Caffrey[e], J.E.Campagne[h], E.Caurier[j], D.Dassié[a], V.Egorov[c], T.Filipova[c,h], R.Gurriaran[a], J.L.Guyonnet[j], F.Hubert[a], Ph.Hubert[a], S.Jullian[h], I.Kisel[c], O.Kochetov[c], V.N.Kornoukhov[g], V.Kovalenko[c], D.Lalanne[h], F.Laplanche[h], F.Leccia[a], I.Linck[j], C.Longuemare[b], Ch.Marquet[a], F.Mauger[b], H.W.Nicholson[i], I.Pilugin[g], F.Piquemal[a], J-L.Reyss[d], X.Sarazin[h], F.Scheibling[j], J.Suhonen[f], C.S.Sutton[i], G.Szklarz[h], V.Timkin[c], R.Torres[a], V.Umatov[g], I.Vanyushin[g], A.Vareille[a], V.Vasilyev[g], Ts.Vylov[c]

[a]CENBG, IN2P3-CNRS et Université de Bordeaux, 33170 Gradignan, France

[b]LPC, IN2P3-CNRS et Université de Caen, 14032 Caen, France

[c]JINR, 141980 Dubna, Russia

[d]CFR, CNRS, 91190 Gif sur Yvette, France

[e]INEEL, Idaho Falls, ID 83415, U.S.A.

[f]JYVÄSKYLÄ University, 40351 Jyväskylä, Finland

[g]ITEP, 117259 Moscow, Russia

[h]LAL, IN2P3-CNRS et Université Paris-Sud, 91405 Orsay, France

[i]MHC, South Hadley, Massachusetts 01075, U.S.A.

[j]IReS, IN2P3-CNRS et Université Louis Pasteur, 67037 Strasbourg, France

[1]Corresponding author, Institute of Theoretical and Experimental Physics, B.Cheremushkinskaya 25, 117259 Moscow, Russia, e-mail: barabash@vxitep.itep.ru, tel.: 007 (095) 129-94-68, fax: 007 (095) 883-96-01.